

Precision of mean-field accretion disc theory and application to standard thin-disc models

Hongzhe Zhou ^{1,2,3*}, Eric G. Blackman ^{2,3†}

¹ *Nordita, KTH Royal Institute of Technology and Stockholm University, Roslagstullsbacken 23, SE-106 91 Stockholm, Sweden*

² *Department of Physics and Astronomy, University of Rochester, Rochester, NY, 14627, USA*

³ *Laboratory for Laser Energetics, University of Rochester, Rochester NY, 14623, USA*

ABSTRACT

Axisymmetric, time-independent accretion disc models are necessarily mean-field theories when applied to turbulent discs since axisymmetry and stationarity apply only upon averaging. Observations with short exposure times represent members in the turbulence ensemble, and comparing with theoretical mean values can falsify the latter only if the theory is additionally supplied with a quantified precision. We previously identified “intrinsic” and “filtering” errors as two contributions to the precision of mean-field theories. Here we generalize to cases where the turbulent scales vary in space. In the geometrically thin, optically thick accretion disc models, disc emission at a given frequency has non-local contributions from the entire disc, and we develop a framework to propagate local fluctuations to the integrated spectrum. In addition, the nonlinear relation between the disc temperature and overall spectrum contributes a systematic “mismatch error” that has not been previously identified. The total error in the calculated disc spectrum is also sensitive to the choice of binning used to compare with data from a telescope of given temporal and spectral resolving powers. For the thin disc example, we show that precision errors are generally small, but vary with emission frequency. In general this means that accurately assessing falsifiability would require a frequency-dependent likelihood function. The thin disc exemplifies our more important purpose: to highlight the need and provide a framework for calculating the imprecision of a mean-field theory.

1 INTRODUCTION

Accretion discs which power the engines of many of the Universe’s most luminous sources, form around compact object like young stars, black holes, and neutron stars when the angular momentum of the in-falling matter cannot be rapidly removed. Accreting systems are observed over a wide range of electromagnetic frequencies, from radio to highly relativistic gamma emission depending on the mass and compactness of the central object. The physics used to model their emission often connects magnetohydrodynamics, radiative processes, plasma physics, and relativity for the most compact engines.

To explain the observed luminosities and light curves of accretion discs, the radial transfer of angular momentum and the energy conversion from gravitational binding to radiation must be more efficient than that can be provided by micro-physical viscosities. The widely used α model, initially proposed by Shakura & Sunyaev (1973), circumvents this problem by considering the dynamics of the mean velocity field and replacing the molecular viscosity by an effective turbulent viscosity. While they did not identify an instability that would lead to this turbulence, a widely invoked mechanism is the magneto-rotational instability as applied to discs (Velikhov 1959; Balbus & Hawley 1991; Hawley & Balbus 1991, 1992; Balbus & Hawley 1992).

The original model by Shakura & Sunyaev (1973) applies to geometrically thin, optically thick discs where the radiative cooling of the gas is efficient, and subsequently, models for radiatively inefficient, geometrically thick discs were

also developed (Shapiro et al. 1976; Abramowicz et al. 1988; Narayan & Yi 1994, 1995a,b). However, all disc models are used with a conceptual inconsistency: on the one hand turbulence is assumed to be the agent of transport, yet at the same time the axisymmetric model is presented as an exact prediction, as if the scale separation between the turbulent eddies and the averaging were infinite when it is not. Mean-field theory itself should be presented with precision error bars associated with the stochastic variability that the turbulence implicit in the enhanced transport causes. In addition, fixed boundary conditions like the mass accretion rate or the disc size are also commonly adopted, but likely unrealistic over a range of time scales.

Strong variability in X-ray fluxes is a persistent feature of accretion-powered X-ray sources (Green et al. 1993; Lawrence & Papadakis 1993; Edelson & Nandra 1999; Markowitz et al. 2003; Vaughan et al. 2003; Uttley & McHardy 2001; McHardy et al. 2004), where the X-ray fluctuation amplitude typically exhibits a power-law relation with the oscillation frequency. Proposed physical origins of this variability include MHD turbulence (Hoshino & Takeshima 1993), a locally fluctuating α parameter (Lyubarskii 1997; Blackman 1998), and mass accretion rate perturbations combined with mass diffusion (Churazov et al. 2001; Kotov et al. 2001; Ingram & Done 2011; Rapisarda et al. 2016; Mushtukov et al. 2018, 2019). There are also attempts to model such variabilities using stochastic processes, for example Burd et al. (2020). These

variabilities highlight that mean-field equations do not tell the full story unless, at minimum, their imprecision is quantified and the accretion rate is allowed to vary.

To facilitate a comparison between mean-field theories and observations, filtering out some of the stochastic variability through repeated, or time averaged, observations of the same object can be helpful. Time averaging is difficult or impossible for objects like active galactic nuclei (AGN) or protoplanetary discs, because their orbital periods and largest turbulent eddy turnover times exceed exposure times. For those cases, spatial averaging somewhat saves the day, as we shall see. In all cases, systematic mismatches between data and mean-field theory predictions must be interpreted properly to determine whether the mean-field theory is falsifiable, or whether the observed deviations from the theory are within the precision error of the theory.

While previous work (e.g., Lyubarskii 1997; Churazov et al. 2001; Ingram & Done 2011) considered *luminosity* oscillations due to changes in mass accretion rates, we aim at quantifying fluctuations about the mean-field value predictions for the disc *spectrum* at all photon frequencies by propagating local disc perturbations with given zeroth-order properties (amplitude, characteristic time, etc.) taken from a mean-field disc model. This is done by quantifying the *precision* of the mean-field theory (Zhou et al. 2018). When integrated over all photon frequencies, the light curve carries over all the temporal characteristics of the fluctuations which allows for a frequency-domain analysis. But more importantly, even just with snapshot observations, it is still meaningful to compare the theoretically predicted fluctuations with spectral data since whether the data falls into the predicted likelihood range determines the *accuracy* of the theory.

In Zhou et al. (2018), we identified two types of (im)precision of a mean-field theory: “intrinsic error” (IE) due to mesoscale fluctuations of turbulence or boundary conditions, and “filtering error” (FE) accounting for the turbulent fluctuations contributing a stochastic imprecision to the predicted observables. In the present paper: (i) We quantify IE and FE for the Shakura-Sunyaev accretion disc model. In so doing, we develop a needed method to account for the imprecision contributions from non-local, and spatially varying fluctuation scales, thereby superseding the local treatment of Blackman et al. (2010). (ii) We newly define and quantify a mismatch error (ME) that arises because certain observables and what mean-field theory predicts for them are not actual the same physical quantity. For example, accretion disc spectra are non-linear in the surface temperature. Thus, spatially averaging the temperature inferred from these spectra a posteriori, is not the same quantity that mean field theory would use as temperature to predict the spectrum a priori.

In Section 2 we introduce the general concepts and framework to calculate the IE, FE and ME for geometrically thin optically thick accretion discs. In Section 3 we apply the method to a thin disc model and quantify the precision of the predicted observed flux. We discuss the implications for falsifiability of the theory when compared to observations in Section 4, and summarize in Section 5.

2 GOALS AND GENERAL FRAMEWORK

Our ultimate goal is to quantify possible deviations of mean-field theory predictions from observed values. In this section and the next, we focus on imprecision associated with the mean-field theory assuming that observations could measure spectra with infinite frequency resolution. We address the discussion of finite resolution in Section 4.

To clarify the idea, we define a snapshot¹ measurement of the spectrum from a spatially unresolved turbulent disc, F_ν^{obs} . We also consider a multi-epoch average (with inter-epoch time longer than the orbit periods at radii considered) of snapshots, assuming each to be drawn from an ensemble \mathcal{D}^{obs} of identical discs with different turbulence realizations but disc turbulence being ergodic. Then we consider this multi-epoch average to be an ensemble average $\langle F_\nu^{\text{obs}} \rangle^{\text{obs}}$; the superscript of the angle brackets means the average is drawn from the ensemble \mathcal{D}^{obs} .

Now suppose that we have a theoretical model that predicts mean-field quantities of a *theoretical* turbulent disc. We call the ensemble associated with this theoretical turbulent disc \mathcal{D}^{th} . How well \mathcal{D}^{obs} coincides with \mathcal{D}^{th} defines the *accuracy* of the theory. Improving accuracy means increasing the fidelity of the input physics. In this work however, we assume that the theoretical mean field model is fully accurate and instead focus on its *precision*.

For a member of \mathcal{D}^{th} , the theory predicts its mean spectrum, F_ν^{th} . For a mean-field theory, F_ν^{th} is the same for all members of \mathcal{D}^{th} , equal to its ensemble average in \mathcal{D}^{th} : $\langle F_\nu^{\text{th}} \rangle^{\text{th}} = F_\nu^{\text{th}}$; here, the superscript of the angle brackets means the average is drawn from \mathcal{D}^{th} . From each element of \mathcal{D}^{th} , we may construct synthetic observations which represent specific predictions processed from the mean-field theory to match what a given telescope would measure. We denote this by $F_\nu^{\text{obs,th}}$. Note that $F_\nu^{\text{obs,th}}$ represents a snapshot measurement of a turbulent disc and so we can also construct the ensemble average $\langle F_\nu^{\text{obs,th}} \rangle^{\text{th}}$. The two quantities F_ν^{th} and $\langle F_\nu^{\text{obs,th}} \rangle^{\text{th}}$ differ in general, and indeed differ for the standard α disc model as we shall see.

Having clarified the notation, the difference between an actual observed value and theoretical mean-field value for the spectrum is

$$\delta F_\nu = F_\nu^{\text{obs}} - F_\nu^{\text{th}} = F_\nu^{\text{obs}} - \langle F_\nu^{\text{obs}} \rangle^{\text{obs}} \quad (1)$$

$$+ \langle F_\nu^{\text{obs}} \rangle^{\text{obs}} - \langle F_\nu^{\text{obs,th}} \rangle^{\text{th}} \quad (2)$$

$$+ \langle F_\nu^{\text{obs,th}} \rangle^{\text{th}} - F_\nu^{\text{th}}, \quad (3)$$

where we have decomposed the right side into three differences: Difference (1) is how much a real observation deviates from its multi-epoch average; difference (2) vanishes if the two ensembles \mathcal{D}^{th} and \mathcal{D}^{obs} are identical, quantifying the accuracy of the theory; difference (3) measures whether the quantity predicted means the same thing as the quantity observations actually measure. We have assumed an accurate

¹ i.e. observation time short compared to the orbit period at disc radii considered. We will not consider long-exposure measurements in this paper, corresponding to many snapshots taken within one orbit time.

Table 1. Different types of averages.

Notation	Meaning
$\mathcal{D}^{\text{obs}}, \langle \cdot \rangle^{\text{obs}}$	ensemble and its associated averages of a real object with different turbulence realizations
$\mathcal{D}^{\text{th}}, \langle \cdot \rangle^{\text{th}}$	ensemble and its associated averages of a theoretical turbulent disc
$\langle \cdot \rangle^{\text{obs}} = \langle \cdot \rangle^{\text{th}} = \langle \cdot \rangle$	for an accurate theory
$\sigma^2(X)$	variance of X in an ensemble
\bar{X}	average used in a mean-field model
X^{obs}	observed value from telescopes
X^{th}	computed value from a mean-field theory
$X^{\text{obs,th}}$	theoretical prediction of a synthetic observation
$X^{\text{obs}} = X^{\text{obs,th}}$	for an accurate theory
$\langle X^{\text{obs}} \rangle^{\text{obs}}$	multi-epoch mean of X^{obs}
$\langle X^{\text{th}} \rangle^{\text{th}} = X^{\text{th}}$	for a mean-field theory
$\langle X^{\text{obs,th}} \rangle^{\text{th}}$	multi-epoch mean of $X^{\text{obs,th}}$

theory, so we set

$$F_\nu^{\text{obs}} = F_\nu^{\text{obs,th}}. \quad (4)$$

Furthermore, we need not distinguish in which ensemble fields are averaged, and use $\langle \cdot \rangle^{\text{obs}} = \langle \cdot \rangle^{\text{th}} = \langle \cdot \rangle$ in what follows. Consequently, Term (2) vanishes. A summary of different types of averages is given in Table 1.

Since δF_ν fluctuates in the ensemble, it will be meaningful to quantify its mean $\langle \delta F_\nu \rangle$ and variance $\sigma^2(\delta F_\nu)$. Using Terms (1) to (3), we define the “filtering error” (FE) as

$$\sigma_{\text{FE}}^2 = \sigma^2 \left(F_\nu^{\text{obs}} - \langle F_\nu^{\text{obs}} \rangle \right) = \sigma^2 \left(F_\nu^{\text{obs}} \right) = \sigma^2 \left(F_\nu^{\text{obs,th}} \right) \quad (5)$$

where the last step comes from our accuracy assumption $F_\nu^{\text{obs}} = F_\nu^{\text{obs,th}}$. The “mismatch error” (ME) is

$$\delta_{\text{ME}} = \left\langle \left\langle F_\nu^{\text{obs,th}} \right\rangle - F_\nu^{\text{th}} \right\rangle = \left\langle F_\nu^{\text{obs,th}} \right\rangle - F_\nu^{\text{th}}. \quad (6)$$

In addition, the error associated with the perturbations in F_ν^{th} induced by varying model parameters (e.g., boundary conditions, transport coefficients) contributes an “intrinsic error” (IE), σ_{IE}^2 . We then have

$$\langle \delta F_\nu \rangle = \delta_{\text{ME}}, \quad (7)$$

$$\sigma^2(\delta F_\nu) = \sigma_{\text{IE}}^2 + \sigma_{\text{FE}}^2. \quad (8)$$

The IE, FE and ME can all be determined theoretically because they only involve F_ν^{th} and $F_\nu^{\text{obs,th}}$, but not F_ν^{obs} . Correspondingly, $F_\nu^{\text{th}} + \langle \delta F_\nu \rangle \pm \sigma(\delta F_\nu)$ will be a mean-field prediction with error bars, giving a finite range of where we expect the observed value F_ν^{obs} to locate. Thus to facilitate a more appropriate comparison between theory and observations than what is commonly done, we must quantify the precision of the former so that the error can be added to the mean and the result compared against an observation when that observation is a member of an ensemble rather than an ensemble average.

For a geometrical thin, optically thick disc, kinetic energy of the flow released from viscous dissipation as material falls inward, is quickly thermalized and a local patch of the disc emits as a black body. The observed emission from each hemisphere will come primarily from an optically thin surface layer. Consider a member from \mathcal{D}^{th} . Let its surface temperature, as if we could measure it, be $T^{\text{obs,th}}$, and the associated

black-body emission per unit area will be

$$f_\nu^{\text{obs,th}} = \frac{2h_P\nu^3/c^2}{e^{h_P\nu/kT^{\text{obs,th}}} - 1}, \quad (9)$$

where h_P is the Planck constant, ν is the photon frequency, c is the speed of light, and k is Boltzmann’s constant. $T^{\text{obs,th}}$ is turbulent and varies with the disc radius r and azimuthal position ϕ , and so does $f_\nu^{\text{obs,th}}$. The observed total power emitted per unit frequency from one side of the disc is then

$$\begin{aligned} F_\nu^{\text{obs,th}} &= \int_0^{2\pi} d\phi \int_{r_*}^{r_{\text{out}}} f_\nu^{\text{obs,th}}(T^{\text{obs,th}}) r dr \\ &\equiv I [T^{\text{obs,th}}], \end{aligned} \quad (10)$$

where r_* and r_{out} are respectively the inner and outer radii of the disc, and I is the spectrum functional. For compact-object accretion engines, typically $r_{\text{out}} \gg r_*$ and r_* is a few times the Schwartzchild radius. Because of the nonlinear dependence on the surface temperature,

$$\left\langle F_\nu^{\text{obs,th}} \right\rangle = \left\langle I [T^{\text{obs,th}}] \right\rangle \neq I \left[\left\langle T^{\text{obs,th}} \right\rangle \right], \quad (11)$$

which is crucial for identifying the ME.

Next we explain what the standard α disc predicts. Commonly, accretion disc theories employ azimuthally and vertically averaged, temporally blurred and density-weighted averaged mean fields. The constructed mean-field equations are solved to obtain a mean surface temperature \bar{T} . The predicted black-body radiation per unit area is then

$$f_\nu^{\text{th}} = \frac{2h_P\nu^3/c^2}{e^{h_P\nu/k\bar{T}} - 1}, \quad (12)$$

and the total emission is

$$F_\nu^{\text{th}} = I [\bar{T}] = \int_0^{2\pi} d\phi \int_{r_*}^{r_{\text{out}}} f_\nu^{\text{th}} r dr = 2\pi \int_{r_*}^{r_{\text{out}}} f_\nu^{\text{th}} r dr. \quad (13)$$

In general $F_\nu^{\text{th}} \neq \langle F_\nu^{\text{obs,th}} \rangle$ given inequality (11), even if $\bar{T} = \langle T^{\text{obs,th}} \rangle$.

Later we derive a probability density function of $T^{\text{obs,th}}$ in the ensemble, so that ensemble averages like those in inequality (11) become calculable. We can then compute the FE from Equation (5), and the ME from Equation (6).

Finally, notice that depending on context, variations in f_ν^{th} may arise for a number of reasons that include variation in the accretion supply rate at the outer disc boundary, and/or

variation—for example via magnetic influence—of the locus of the inner disc radius where most of the luminosity originates. Here we focus only on IE from variations in F_ν^{th} arising from f_ν^{th} , and not from the size of the integrated region.

In the subsequent subsections we formulate the three error contributions. We do this by considering local perturbations introduced to f_ν^{th} or $f_\nu^{\text{obs,th}}$, and then propagate those to F_ν^{th} or $F_\nu^{\text{obs,th}}$. We start from the IE.

2.1 Intrinsic error

We focus on the contribution to the IE from fluctuations in the mean accretion rate \dot{m} whose correlation time scale is much shorter than the accretion time scale. That \dot{m} is azimuthally averaged ensures that the variation in \dot{m} is homogeneous over an annulus, and these fluctuations gradually “propagate” inward.

The variance of the local emission f_ν^{th} can be calculated by propagating the variance of \dot{m} ,

$$\sigma^2(f_\nu^{\text{th}}) = \left(\frac{\partial f_\nu^{\text{th}}}{\partial \dot{m}} \right)^2 \sigma^2(\dot{m}), \quad (14)$$

and the fluctuation of f_ν^{th} has a correlation length, say, l_r in the radial direction as a consequence of the inwardly moving fluctuation of \dot{m} . In general, l_r depends on r .

Propagating $\sigma^2(f_\nu^{\text{th}})$ to $\sigma^2(F_\nu^{\text{th}})$ [related by Equation (13)] is non-trivial. Intuitively, smaller l_r implies smaller $\sigma^2(F_\nu^{\text{th}})$, because contributions from uncorrelated fluctuating parts rapidly cancel out. In Appendix A, we derive the propagation formula which applies when the correlation length is much smaller than the region being integrated, and thus applies for the thin disc when $l_r \ll r_{\text{out}}$. Given the axisymmetry of \dot{m} and f_ν^{th} , we use the one-dimensional formula Equation (A18), which yields

$$\begin{aligned} \sigma^2(F_\nu^{\text{th}}) &= 4\pi^2 \int_{r_*}^{r_{\text{out}}} \sigma^2(f_\nu^{\text{th}}) l_r r^2 dr \\ &= 4\pi^2 \sigma^2(\dot{m}) \int_{r_*}^{r_{\text{out}}} \left(\frac{\partial f_\nu^{\text{th}}}{\partial \dot{m}} \right)^2 l_r r^2 dr, \end{aligned} \quad (15)$$

where the last equality follows for constant $\sigma^2(\dot{m})$ at $r = r_{\text{out}}$.

If the surface temperature \bar{T} obeys a conventional power law relation $\bar{T} \propto \dot{m}^p$, then the intrinsic error σ_{IE} induced by variations in \dot{m} can be determined via

$$\sigma_{\text{IE}}^2 \equiv \sigma^2(F_\nu^{\text{th}}) = 4\pi^2 p^2 \tilde{\sigma}_{\dot{m}}^2 \int_{r_*}^{r_{\text{out}}} \bar{T}^2 \left(\frac{\partial f_\nu^{\text{th}}}{\partial \bar{T}} \right)^2 l_r r^2 dr, \quad (16)$$

where $\tilde{\sigma}_{\dot{m}} = \sigma(\dot{m})/\dot{m}$ is the relative variance of the mean accretion rate.

2.2 Filtering error

The FE arises when observations represent an ensemble member rather than ensemble mean. To calculate the FE, we first model the ensemble \mathcal{D}^{th} by constructing the associated probability distribution functions (PDFs). The luminosity L_{ed} of a single eddy constantly brightens and dims, and we assume a uniformly PDF for L_{ed} :

$$P_{L_{\text{ed}}}(x) = \frac{1}{2\bar{L}}, \quad 0 \leq x \leq 2\bar{L}, \quad (17)$$

so that $P_{L_{\text{ed}}}(x)dx$ is the probability to find L_{ed} between x and $x + dx$. Here \bar{L} is the mean of L_{ed} , and equals the luminosity of the mean-field disc model from an area equal to that of the eddy. In general, \bar{L} depends on the disc radius in a mean-field model, and so does $P_{L_{\text{ed}}}$. As a possible extension, PDFs drawn from direct numerical simulations (e.g. Lee & Gammie 2020) may also be used.

For optically thick discs where surface eddies emit blackbody spectra, $L_{\text{ed}} = \sigma_{\text{SB}} T^4$, where σ_{SB} is the Stefan-Boltzmann constant. We can then write the PDF of T as

$$P_T(x) = \frac{2x^3}{\bar{T}^4}, \quad 0 \leq x \leq 2^{1/4}\bar{T}, \quad (18)$$

where $\bar{T} = (\bar{L}/\sigma_{\text{SB}})^{1/4}$. Equation (18) can be used to calculate the ensemble variance of $f_\nu^{\text{obs,th}}$, via

$$\sigma^2(f_\nu^{\text{obs,th}}) = \langle f_\nu^{\text{obs,th}2} \rangle - \langle f_\nu^{\text{obs,th}} \rangle^2, \quad (19)$$

where

$$\langle Q \rangle = \int_0^{2^{1/4}\bar{T}} Q(x) P_T(x) dx \quad (20)$$

is the ensemble average of quantity Q , approximately equal to its multi-epoch averaged observational value. The fluctuation of $f_\nu^{\text{obs,th}}$ is due to turbulence with an assumed isotropic correlation length of eddy scale l_{ed}^2 .

To propagate the precision of $f_\nu^{\text{obs,th}}$ to that of $F_\nu^{\text{obs,th}}$ [related via Equation (10)], we use the two-dimensional formula of Equation (A22) in Appendix A, since $f_\nu^{\text{obs,th}}$ is turbulent on the disc surface. Combining with Equation (10) we obtain

$$\sigma_{\text{FE}}^2 = \sigma^2(F_\nu^{\text{obs,th}}) = 2\pi \int_{r_*}^{r_{\text{out}}} \sigma^2(f_\nu^{\text{obs,th}}) l_{\text{ed}}^2 r dr. \quad (21)$$

2.3 Mismatch error

Since the spectrum depends nonlinearly on the surface temperature, the ensemble average of the spectrum taken as a function of the total fields is not the same as the spectrum taken as a function of the ensemble averaged fields as per Equation (11). The associated ME, using equation (20), is

$$\delta_{\text{ME}} = \int_0^{2\pi} d\phi \int_{r_*}^{r_{\text{out}}} \left(\langle f_\nu^{\text{obs,th}} \rangle - f_\nu^{\text{th}} \right) r dr. \quad (22)$$

3 APPLICATION TO STANDARD THIN DISC MODELS

3.1 The disc model

For a geometrical thin, optically thick disc, the power emitted per unit frequency per unit time from an area $r dr d\phi$ from the disc is

$$dF_\nu = \frac{2h_P \nu^3 / c^2}{e^{h_P \nu / kT} - 1} r dr d\phi. \quad (23)$$

Integrating over the whole disc and taking into account the inclination angle i of the disc and its distance D from the observer, we get the radiation flux, namely, the received power

² This can be relaxed in generalized extensions.

per unit frequency per unit time per unit receiving area

$$F_\nu = \frac{\cos i}{D^2} \int_0^{2\pi} d\phi \int_{r_*}^{r_{\text{out}}} \frac{2h_P \nu^3 / c^2}{e^{h_P \nu / kT} - 1} r dr d\phi. \quad (24)$$

As an example disc structure, we employ what was used for protoplanetary discs in Edgar et al. (2007). In this mean-field theory, mean-field quantities are indicated by an overline and the detailed disc structure is governed by the following:

(i) The ratio of disc scale height h to radius r is small, approximately $h/r \sim 0.01$ with small dependence on r . The disc mass is also much smaller than that of the central object so the gravity from the latter dominates. Vertical hydrostatic equilibrium gives the relation

$$\frac{GM\rho h}{r^2} \frac{h}{r} \simeq P \Rightarrow c_S = \Omega_K h, \quad (25)$$

where G is the gravitational constant, M the mass of the young star, ρ is the gas density, $c_S = \sqrt{P/\rho}$ is the sound speed, and $\Omega_K = \sqrt{GM/r^3}$ is the Keplerian speed.

(ii) The turbulent viscosity $\nu_T \simeq v_{\text{ed}} l_{\text{ed}}$ is parameterized by an α prescription (Shakura & Sunyaev 1973), namely $\nu_T = \alpha c_S h$ where α is a dimensionless constant. The eddy scales can be estimated by $v_{\text{ed}} = \alpha^{1/2} c_S$ and $l_{\text{ed}} = \alpha^{1/2} h$, and $\tau_{\text{ed}} = h/c_S = \Omega_K^{-1}$. Common values of α from numerical simulations vary from ~ 0.01 for thin discs to ~ 0.3 for thicker ones (Stone et al. 1996; Hawley & Krolik 2001; Sano et al. 2004; Nauman & Blackman 2014), in rough agreement with observations (King et al. 2007; Kotko & Lasota 2012; Rafikov 2017; Ansdell et al. 2018; Flaherty et al. 2020) although questions about convergence, and the dependence on geometry, initial conditions, and dissipation persist (e.g. Hawley et al. 1995; Sorathia et al. 2012; Bodo et al. 2014; Shi et al. 2016; Nauman & Blackman 2017). Nevertheless, we choose $\alpha = 0.01$ and 0.3 as representative example values.

(iii) The equations of mass and angular momentum transport yield a relation between the mean mass accretion rate \dot{m} , the surface density Σ , and the turbulent viscosity ν_T ,

$$\dot{m} = 3\pi \Sigma \nu_T. \quad (26)$$

(iv) The temperature \bar{T}_c at the mid plane of the disc is related to the sound speed via

$$\frac{3}{2} k \bar{T}_c = \bar{\rho} c_S^2, \quad (27)$$

where $\bar{\rho}$ is the mean density. The surface temperature \bar{T} is related to the central temperature via the optical depth τ from the mid plane to the surface by

$$\bar{T}_c^4 = \frac{3}{8} \tau \bar{T}^4, \quad (28)$$

and the optical depth is given by the constant opacity κ via

$$\tau = \frac{1}{2} \kappa \Sigma. \quad (29)$$

(v) The energy emitted through the surface is

$$\frac{9}{8} \Sigma \Omega_K^2 \nu_T = \epsilon \sigma_{\text{SB}} \bar{T}^4, \quad (30)$$

where ϵ is a constant emissivity.

Solving these disc equations yields

$$h = h_* \tilde{r}^{21/20}, \quad h_* \propto M^{-7/20} \dot{m}^{1/5} \alpha^{-1/10}, \quad (31)$$

$$\bar{T} = \bar{T}_* \tilde{r}^{-21/40}, \quad \bar{T}_* \propto M^{7/40} \dot{m}^{3/20} \alpha^{1/20}, \quad (32)$$

$$c_S = c_{S*} \tilde{r}^{-9/20}, \quad c_{S*} \propto M^{3/20} \dot{m}^{1/5} \alpha^{-1/10}, \quad (33)$$

where we have used a subscript asterisk to denote quantities at the inner radius r_* of the disc, and $\tilde{r} = r/r_*$. We denote $\theta \equiv h_*/r_*$ as the height-to-radius ratio at the inner edge of the disc. Equation (32) tells us that $p = \partial \ln \bar{T} / \partial \ln \dot{m} = 3/20$. This will be used in Equation (16).

3.2 Non-dimensionalization

To simplify calculations we will work with dimensionless quantities. The fiducial unit of temperature is chosen to be \bar{T}_* , the mean surface temperature measured at $r = r_*$. The dimensionless photon energy is then

$$\beta = \frac{h_P \nu}{k \bar{T}_*}. \quad (34)$$

We will also use r_* as the fiducial length unit.

Non-dimensionalizing Equations (23) and (24) we obtain the dimensionless emitted powers per unit frequency per unit emitting area

$$f_\nu^{\text{obs,th}}(T) = \frac{\beta^3}{e^{\beta/(T/\bar{T}_*)} - 1}, \quad (35)$$

$$f_\nu^{\text{th}}(\bar{T}) = \frac{\beta^3}{e^{\beta/(\bar{T}/\bar{T}_*)} - 1}. \quad (36)$$

From the temperature derivative of the latter, we also obtain

$$\bar{T}^2 \left(\frac{\partial f_\nu^{\text{th}}}{\partial \bar{T}} \right)^2 = \frac{e^{2\beta/(\bar{T}/\bar{T}_*)} f_\nu^{\text{th}4}}{\beta^4 (\bar{T}/\bar{T}_*)^2}, \quad (37)$$

to be used for calculating the IE in Equation (16).

The corresponding dimensionless flux from the entire disc is

$$F_\nu^{\text{obs,th}} = \int_0^{2\pi} d\phi \int_1^R f_\nu^{\text{obs,th}}(T) \tilde{r} d\tilde{r}, \quad (38)$$

$$F_\nu^{\text{th}} = 2\pi \int_1^R f_\nu^{\text{th}}(\bar{T}) \tilde{r} d\tilde{r}, \quad (39)$$

where $R = r_{\text{out}}/r_*$.

The formulae for calculating precision in Appendix A will also be non-dimensionalized: specifically, the length scales will be measured in units of r_* .

3.3 Calculation of the intrinsic error

We assume that the time scale τ_{acc} of the variation in \dot{m} is shorter than or comparable to the accretion time scale, otherwise matter can accrete before experiencing much influence from the perturbation, and F_ν^{th} simply changes adiabatically with \dot{m} .

In the radial direction, the accretion speed is

$$v_r = \frac{3\nu_t}{2r} = \frac{3l_{\text{ed}}^2}{2r\tau_{\text{ed}}} = \frac{3}{2} \alpha \theta^2 \tilde{r}^{-2/5} v_{K*}, \quad (40)$$

so the typical correlation length of the fluctuations in \dot{m} will be

$$l_{\text{acc}} = v_r \tau_{\text{acc}} \Rightarrow \frac{l_{\text{acc}}}{r_*} = \frac{3}{2} \Omega_{K*} \tau_{\text{acc}} \alpha \theta^2 \tilde{r}^{-2/5}. \quad (41)$$

Using Equations (16) and (37) with lengths in units of r_* ,

$$\begin{aligned}\sigma_{\text{IE}}^2 &= 4\pi^2 p^2 \tilde{\sigma}_m^2 \int_1^R \frac{e^{2\beta/(\bar{T}/\bar{T}_*)} f_\nu^{\text{th}4} l_{\text{acc}}}{\beta^4 (\bar{T}/\bar{T}_*)^2 r_*} \tilde{r}^2 d\tilde{r} \\ &= 6\pi^2 p^2 \tilde{\sigma}_m^2 \Omega_{K_*} \tau_{\text{acc}} \alpha \theta^2 \beta^8 \int_1^R \frac{e^{2\beta\tilde{r}^{21/40}} \tilde{r}^{53/20}}{(e^{\beta\tilde{r}^{21/40}} - 1)^4} d\tilde{r}. \quad (42)\end{aligned}$$

The relative IE measured in $\tilde{\sigma}_m$ is therefore

$$\begin{aligned}\frac{\sigma_{\text{IE}}/F_\nu^{\text{th}}}{\tilde{\sigma}_m} &= \frac{3\sqrt{6}}{40} (\Omega_{K_*} \tau_{\text{acc}})^{1/2} \alpha^{1/2} \theta \beta \\ &\times \frac{\left[\int_1^R e^{2\beta\tilde{r}^{21/40}} (e^{\beta\tilde{r}^{21/40}} - 1)^{-4} \tilde{r}^{53/20} d\tilde{r} \right]^{1/2}}{\int_1^R (e^{\beta\tilde{r}^{21/40}} - 1)^{-1} \tilde{r} d\tilde{r}}. \quad (43)\end{aligned}$$

The IE scales as $\tau_{\text{acc}}^{1/2}$ and increases with increasing τ_{acc} , until the approximation $l_{\text{acc}} \ll r_{\text{out}}$ (used in Appendix A) fails. Then the standard disc model is also invalidated because the mean accretion rate over the disc varies on a length scale comparable to r_{out} .

For typical values $\Omega_{K_*} \tau_{\text{acc}} = 1000$, $\theta = 0.01$, $\alpha = 0.05$, and $R = 10^2, 10^3, 10^4$, the relative IE (normalized by $\tilde{\sigma}_m$) is plotted in panel (a) of Figure 1. At fixed $\tilde{\sigma}_m$, larger discs have lower relative imprecision at low frequency because a larger fractional contribution comes from the outer disc where the correlation length of fluctuations is small due to a smaller accretion speed.

3.4 Calculation of the mismatch error

Using Equation (18), the PDF of the total surface temperature T is

$$\begin{aligned}P_T(x) &= \frac{2x^3}{\bar{T}^4} = \frac{2x^3}{\bar{T}_*^4} \tilde{r}^{-21/10}, \\ &\text{for } 0 \leq x \leq 2^{1/4} \bar{T} = 2^{1/4} \bar{T}_* \tilde{r}^{-21/40}. \quad (44)\end{aligned}$$

This PDF has a radial dependence because \bar{T} is a function of r . It is then straightforward to calculate

$$\langle f_\nu^{\text{obs,th}} \rangle = 2\beta^3 \tilde{r}^{21/10} \int_0^{2^{1/4} \tilde{r}^{-21/40}} \frac{x^3 dx}{e^{\beta/x} - 1}. \quad (45)$$

We now compute the mean total flux for this model and compare it with the theoretical prediction F_ν^{th} . Integrating $\langle f_\nu^{\text{obs,th}} \rangle$ over the whole disc and using Equation (22) we obtain

$$\frac{\delta_{\text{ME}}}{F_\nu^{\text{th}}} = \frac{2 \int_1^R \left(\int_0^{2^{1/4} \tilde{r}^{-21/40}} \frac{x^3 dx}{e^{\beta/x} - 1} \right) \tilde{r}^{31/10} d\tilde{r}}{\int_1^R (e^{\beta\tilde{r}^{21/40}} - 1)^{-1} \tilde{r} d\tilde{r}} - 1, \quad (46)$$

as plotted in panel (c) of Figure 1.

We remind that δ_{ME} reflects the disagreement between F_ν^{th} and $\langle f_\nu^{\text{obs,th}} \rangle$ that arises from comparing the following two theoretical approaches: (i) First solve for mean fields such as the disc temperature \bar{T} , and then calculate the disc spectrum as given by $F_\nu^{\text{th}}(\bar{T})$; (ii) Solve for both the mean and the fluctuation in temperature (possibly statistically) and combine to obtain total temperature T , then calculate the associated total spectrum, and then take the average to get $\langle F_\nu^{\text{obs,th}} \rangle$. Approach (i) is commonly adopted by theorists, whereas approach (ii) would be used by theorists to more accurately compare to what observations measure.

The magnitude of δ_{ME} depends on the choice of PDF for T , and for different PDFs we may get either smaller or larger values. But our main purpose here is to clarify the concept δ_{ME} itself, and what a mean-field theory predicts.

3.5 Calculation of the filtering error

In order to quantify the FE [Equations (5) and (21)], we need to calculate the variance of $f_\nu^{\text{obs,th}}$. From Equation (44) we get

$$\langle f_\nu^{\text{obs,th}2} \rangle = 2\beta^6 \tilde{r}^{21/10} \int_0^{2^{1/4} \tilde{r}^{-21/40}} \frac{x^3 dx}{(e^{\beta/x} - 1)^2}, \quad (47)$$

and together with Equation (45), we have

$$\begin{aligned}\sigma^2 (f_\nu^{\text{obs,th}}) &= 2\beta^6 \tilde{r}^{21/10} \left[\int_0^{2^{1/4} \tilde{r}^{-21/40}} \frac{x^3 dx}{(e^{\beta/x} - 1)^2} \right. \\ &\quad \left. - 2\tilde{r}^{21/10} \left(\int_0^{2^{1/4} \tilde{r}^{-21/40}} \frac{x^3 dx}{e^{\beta/x} - 1} \right)^2 \right]. \quad (48)\end{aligned}$$

Applying Equation (21) (again, lengths are measured in r_*) we get

$$\begin{aligned}\sigma_{\text{FE}}^2 &= 2\pi \int_1^R \sigma^2 (f_\nu^{\text{obs,th}}) \left(\frac{l_{\text{ed}}}{r_*} \right)^2 \tilde{r} d\tilde{r} \\ &= 4\pi \alpha \theta^2 \beta^6 \int_1^R \left[\int_0^{2^{1/4} \tilde{r}^{-21/40}} \frac{x^3 dx}{(e^{\beta/x} - 1)^2} \right. \\ &\quad \left. - 2\tilde{r}^{21/10} \left(\int_0^{2^{1/4} \tilde{r}^{-21/40}} \frac{x^3 dx}{e^{\beta/x} - 1} \right)^2 \right] \tilde{r}^{26/5} d\tilde{r}. \quad (49)\end{aligned}$$

The relative FE is therefore

$$\begin{aligned}\frac{\sigma_{\text{FE}}}{F_\nu^{\text{th}}} &= \sqrt{\frac{\alpha \theta^2}{\pi}} \left[\int_1^R (e^{\beta\tilde{r}^{21/40}} - 1)^{-1} \tilde{r} d\tilde{r} \right]^{-1} \\ &\times \left\{ \int_1^R \left[\int_0^{2^{1/4} \tilde{r}^{-21/40}} \frac{x^3 dx}{(e^{\beta/x} - 1)^2} \right. \right. \\ &\quad \left. \left. - 2\tilde{r}^{21/10} \left(\int_0^{2^{1/4} \tilde{r}^{-21/40}} \frac{x^3 dx}{e^{\beta/x} - 1} \right)^2 \right] \tilde{r}^{26/5} d\tilde{r} \right\}^{1/2}. \quad (50)\end{aligned}$$

For typical values $\theta = 0.01$, $\alpha = 0.05$, and $R = 10^3, 10^4, 10^5$, the relative FE is plotted in panel (b) of Figure 1. Notably the relative FE is small for thin discs, primarily because of the large number of eddies in the disc: the eddy scale is $l_{\text{ed}} \sim \alpha^{1/2} h \sim \alpha^{1/2} \theta r$ and both α and θ are very small.

3.6 The total imprecision and the luminosity fluctuation

Assuming the IE and FE are independent contributors, their total contribution to the imprecision of the theory is

$$\sigma^2 = \sigma_{\text{IE}}^2 + \sigma_{\text{FE}}^2. \quad (51)$$

For $\tilde{\sigma}_m = 1$, the theoretical value F_ν^{th} and the theoretically predicted observational value $\langle F_\nu^{\text{obs,th}} \rangle = F_\nu^{\text{th}} + \delta_{\text{ME}}$, along with $F_\nu^{\text{obs,th}} \pm \sigma$ are plotted in panel (d) of Figure 1. The precision error from σ is generally small for thin discs studied here, but can be significantly larger for thick discs.

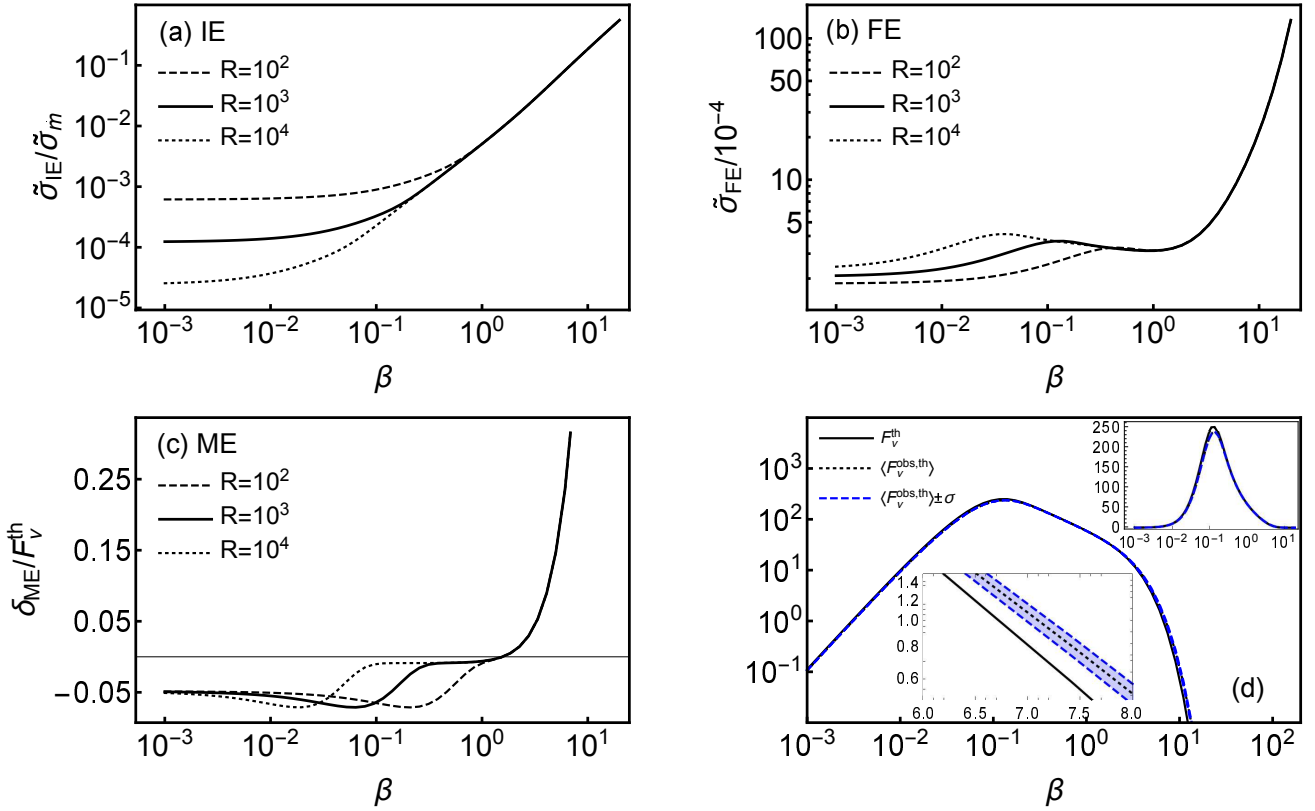


Figure 1. The relative intrinsic error normalized by $\tilde{\sigma}_m$ [panel (a)], relative filtering error [panel (b)], relative mismatch error [panel (c)], and the theoretical predictions of the disc spectrum F_ν^{th} and $\langle F_\nu^{\text{obs,th}} \rangle$ with the total error $\sigma = \sqrt{\sigma_{IE}^2 + \sigma_{FE}^2}$ of the mean-field model [panel (d)]. The chosen disc parameters are $\Omega_{K*}\tau_{\text{acc}} = 10^3$, $\theta = 0.01$, $\alpha = 0.05$ for all panels, outer radius $R = 10^2, 10^3, 10^4$ for panels (a), (b) and (c). For panel (d), we have used $R = 10^3$ and $\tilde{\sigma}_m = 1$, and the insets show zoom-in's at high photon frequencies and log-linear-scale plots.

The relative difference in luminosities that result from integrating F_ν^{th} and $\langle F_\nu^{\text{obs,th}} \rangle$ is 0.0016% at $\alpha = 0.05$, and in the most extreme cases where the whole disc brightens or dims coherently, the relative fluctuation around the ensemble-averaged luminosity is 0.42% for $\alpha = 0.01$, and 2.35% for $\alpha = 0.3$.

4 OBSERVATIONS AND FALSIFIABILITY

So far we have focused on the imprecision that results from a mean-field theory. To quantify the effect of this imprecision on the falsifiability of the theory, we must also consider the spectral resolving power of a given telescope.

Focusing on spatially unresolved objects, we note that data from longer duration observations are more appropriate for comparing to a mean-field theory whereas snapshot observations are expected to exhibit more fluctuations around the mean. High temporal resolution data from a telescope can be binned for optimal comparison with a mean-field theory. In what follows we consider short exposure times and the effect of different telescope frequency resolutions.

Consider the spectral resolving power of a telescope,

$$\text{RP} = \frac{\beta}{\Delta\beta}, \quad (52)$$

where $\Delta\beta$ is the resolving bandwidth at photon frequency β .

For snapshot measurements where the exposure time τ_{exp} is much smaller than the fluctuation timescales $\tau_{\text{IE,FE}}$ (which we estimate in Appendix B), the observed flux is

$$F_\nu^{\text{T}}(\beta) = \frac{\text{RP}}{\beta} \int_{\beta}^{\beta(1+\text{RP}^{-1})} F_\nu^{\text{obs,th}}(\beta') d\beta'. \quad (53)$$

As for the expected fluctuation of F_ν^{T} at this resolution, if the telescope does not resolve the largest coherent frequency width associated with the model (i.e., $\text{RP} < \beta/\Delta\beta_{\text{IE,FE}}$), we obtain

$$\sigma_{\text{E}}^{\text{T}} \simeq \left(\frac{\text{RP}}{\beta} \right) \left[\int_{\beta}^{\beta(1+\text{RP}^{-1})} \sigma_{\text{E}}^2(\beta') \Delta\beta'_s d\beta' \right]^{1/2}, \quad (54)$$

where E=IE or FE, and their respective coherent frequency widths $\Delta\beta_{\text{E}}$, i.e., the β range over which fluctuations are expected to be coherent, are estimated from the spatial coherent scale and given in Appendix B. For large RP, the errors simply become the fully resolved ones, i.e., σ_{IE} and σ_{FE} .

In Figure 2, we plot the total relative precision for different RP. For each case, the vertical lines in corresponding colors indicate the photon frequency above which the resolving power exceeds the corresponding coherent frequency widths associated with the model, thereby delineating the transition from low to high RP regimes. Smaller RP reduces the effect of fluctuations (as in the low- β cases) because more fluctuation cells are averaged within a single resolving bandwidth.

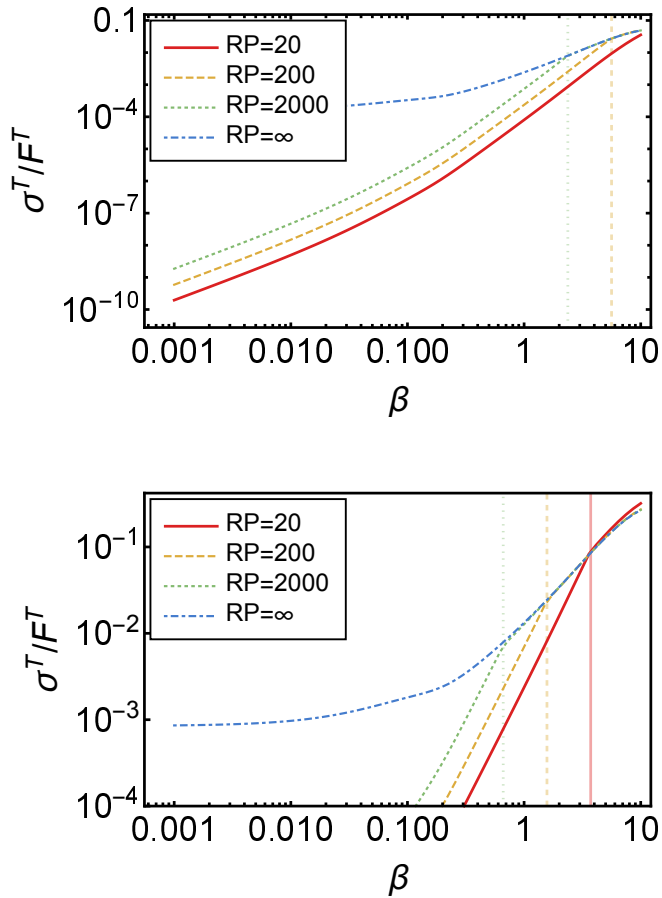


Figure 2. The total relative fluctuation of snapshot measurements from the IE and FE, with $\tilde{\sigma}_{\dot{m}} = 1$, $\Omega_{K*}\tau_{\text{acc}} = 10^3$, $\theta = 0.01$, $R = 10^3$, and $\alpha = 0.01$ (top) and 0.3 (bottom). In all cases, the IE is about 100 times the FE. The vertical lines show the photon frequencies above which the resolving power exceeds the coherent frequency widths associated with the model.

This rule breaks down when the spectrum is so steep that the error in F_{ν}^T becomes large and dominates the relative error (as in the high- β cases). The optimal RP to minimize the error depends on both the disc and the fluctuation models.

The potentially high contribution to the error as shown for example in the lower panel of Figure 2, reflects that when fitting turbulent spectra, the inferred model may fail to match those from an accurate theory, or misleadingly appear to agree with an inaccurate theory, if fluctuations around mean-field results are not properly estimated. Quantifying precision of mean-field theories is necessary to assess their falsifiability. Our disc example shows that accurate falsification may require a likelihood function or data weighting that reflects the fidelity of the theoretical mean-field values in different regions of the parameter space (e.g. frequency, in the disc example).

5 CONCLUSION

We extended the precision-of-mean-field-theory framework developed in Zhou et al. (2018) and exemplified its application to accretion disc theory, specifically focusing on a geometrically thin, optically thick disc. In our formalism as

presently applied, the IE originates from perturbations to the accretion rate, the FE arises from the turbulent nature of the disc, and the ME is due to the nonlinear dependence of the disc spectrum on the surface temperature. We modeled the fluctuations in basic physical quantities such as turbulent velocity and temperature as local functions of r and ϕ , and assigned them with spatially varying correlation lengths. The consequent fluctuations of global quantities, namely spectra and luminosity, were then derived. Intuitive expectation from the central limit theorem is that the more fluctuations over which we average the less the fluctuations contribute to imprecision. This is indeed verified after carefully taking the spatially varying small-scale correlation scales into consideration.

We then binned the calculated spectra and imprecision to account for finite telescope RP. A lower RP improves precision when the coherent frequency bandwidth is not resolved, while the situation is reversed once the RP exceeds the coherent frequency width of the model. The resulting fluctuations of synthetic observations are small for thin discs but would become non-negligible for thicker discs at high photon frequencies. Regardless of the specific numerical values, the key point here is that a mean-field theory is only falsifiable when its precision is properly calculated and taken into account in model testing (e.g., Liu et al. 2008) or data fitting.

We have considered only the thermal emission spectrum for thin discs. For coronae and thick discs, cooling can be less efficient and densities lower, and overall, non-thermal radiation is more important, if not dominant. One set of thick disc models is the advection-dominated accretion disc models (ADAFs; Narayan & Yi 1994, 1995a,b). We leave the generalized calculation of precision of the ADAF models for future work. Since X-ray binaries seem to exhibit transitions between geometrically thick and geometrically thin discs, ultimately combining calculations for thick and thin discs here will be useful, if not essential, for computing the precision during all observed states of these systems.

Our precision analysis so far does not distinguish the time scale of each fluctuation cell other than allowing distinct universal time scales for IE and FE respectively (τ_{acc} for IE and τ_{ed} for FE). A future generalization of the method, either for IE or FE, would be to allow the perturbations from turbulence or that vary \dot{m} to be composed of different time scales, such as a turbulent flow with a continuous spectrum. This may ultimately be related to variabilities of X-ray emitters. We also leave this for future work.

ACKNOWLEDGEMENTS

We thank Jing Yang and Alexandra Veledina for useful discussions. HZ acknowledges support from Horton Fellowship from the Laboratory for Laser Energetics at U. Rochester. EB acknowledges support from NSF grants AST-1813298, PHY-2020249; DOE grants DE-SC0020432 and DE-SC0020103; KITP UC Santa Barbara funded by NSF Grant PHY-1748958.

APPENDIX A: PROPAGATING PRECISION TO INTEGRATED QUANTITIES

To determine the precision of mean-field theories, we often need to compute the variance of an integrated quantity from the local variance and correlation length. For example, consider a one dimensional case,

$$K = \int_a^b k(r) dr \quad (\text{A1})$$

where k is some turbulent field drawn from an ensemble with correlation length $l(r) \ll b - a$ and variance $\sigma^2(k)$. Both $l(r)$ and $\sigma^2(k)$ are smooth functions of r , modelled by some mean-field theory. Here we provide two methods to derive the variance of K .

Method 1: Let us rewrite K as the sum of contributions from fluctuating cells. We may divide the system into grids with the size of the i th cell being $l_i \equiv l(r_i)$, and the grid can be constructed in the following way:

$$r_1 = a, r_{i+1} = r_i + l_i, i = 1, 2, \dots \quad (\text{A2})$$

Now K is given by

$$K = \int_a^b k(r) dr \simeq \sum_i k_i l_i, \quad (\text{A3})$$

where $k_i = k(r_i)$. The mean of K^2 is

$$\langle K^2 \rangle = \sum_{i,j} \langle k_i k_j \rangle l_i l_j. \quad (\text{A4})$$

Since each cell varies independently, we have

$$\begin{aligned} \langle k_i k_j \rangle &= \begin{cases} \langle k_i \rangle \langle k_j \rangle, & i \neq j \\ \langle k_i^2 \rangle, & i = j \end{cases} \\ &= \langle k_i \rangle \langle k_j \rangle + \delta_{ij} (\langle k_i^2 \rangle - \langle k_i \rangle \langle k_j \rangle). \end{aligned} \quad (\text{A5})$$

Thus

$$\begin{aligned} \langle K^2 \rangle &= \sum_{i,j} \langle k_i \rangle \langle k_j \rangle l_i l_j + \sum_i \sigma^2(k_i) l_i^2 \\ &= \langle K \rangle^2 + \sum_i \sigma^2(k_i) l_i^2 \\ &\simeq \langle K \rangle^2 + \int_a^b \sigma^2(k) l(r) dr, \end{aligned} \quad (\text{A6})$$

where the last step we have used one of the l_i 's as the line element, valid when $l(r) \ll r$. The variance of K is thus

$$\sigma^2(K) = \langle K^2 \rangle - \langle K \rangle^2 \simeq \int_a^b \sigma^2(k) l(r) dr. \quad (\text{A7})$$

Method 2: Consider a coarse-grained field

$$k'(r) = \int_a^b k(r-s) G_{c(r)}(s) ds \quad (\text{A8})$$

and the corresponding integral

$$K' = \int_a^b k'(r) dr. \quad (\text{A9})$$

Here $G_c(s)$ is a normalized kernel with compact support from $|s| \leq c$ where c is a function of r , satisfying $l(r) \ll c(r) \ll$

$b - a$. We then have

$$\begin{aligned} K' &= \int_a^b G_{c(r)}(s) ds \int_a^b k(r-s) dr \\ &= \int_a^b G_{c(r)}(s) ds \int_{a-s}^{b-s} k(r) dr \\ &\simeq \int_a^b G_{c(r)}(s) ds \int_a^b k(r) dr = K. \end{aligned} \quad (\text{A10})$$

The last equality follows the normalization property of G . Thus, we only need to quantify the variance of K' .

The coarse-grained field k' locally has a Gaussian distribution because of the central limit theorem. For each averaging cell of size $c(r)$, the number of fluctuating cells of size $l(r)$ is $c(r)/l(r)$, and therefore

$$\sigma^2(k') = \frac{\sigma^2(k)}{c(r)/l(r)}. \quad (\text{A11})$$

Now we divide the region $a \leq r \leq b$ into grids, constructed by

$$r_1 = a, r_{i+1} = r_i + c_i, i = 1, 2, \dots, \quad (\text{A12})$$

where $c_i = c(r_i)$. Since $c(r) \ll b - a$, K' can be approximated by

$$K' = \sum_i k'_i c_i, \quad (\text{A13})$$

and since each k'_i is a Gaussian, the variance of K' , which is equal to that of K , is given by

$$\begin{aligned} \sigma^2(K) &= \sigma^2(K') \\ &= \sum_i \sigma^2(k'_i) c_i^2 = \sum_i \frac{\sigma^2(k_i)}{c_i/l_i} c_i^2 = \sum_i \sigma^2(k_i) l_i c_i \\ &\simeq \int_a^b \sigma^2(k) l(r) dr, \end{aligned} \quad (\text{A14})$$

which agrees with Method 1.

Equation (A14) can be tested numerically. We choose $a = 1$, $b = 100, 200, 300, 500$, $l(r) = 0.05r^{1/2}$, and

$$\sigma^2(k) = \frac{r^3 e^{0.1\sqrt{r}}}{(e^{0.1\sqrt{r}} - 1)^4}. \quad (\text{A15})$$

A multi-dimensional covariance matrix

$$G_{ij} = \sigma^2(k(r')) e^{-\frac{(r_i - r_j)^2}{l(r')/2}}, r' = \min(r_i, r_j) \quad (\text{A16})$$

is prescribed for all pairs of $r_{i,j}$ on a discretized grid of $r \in [a, b]$, based on which the field is assigned stochastically and repeatedly in an ensemble of size 256. Figure A1 shows the comparison between the numerical and theoretical results.

We summarize the following rules for propagating precision to an integrated quantity from its integrand:

- (i) Keep the line element of the integration unchanged.
- (ii) Replace the integrand by the variance of the integrand multiplied by the correlation length in the relevant direction.

As an example on a disc surface, suppose K is given by

$$K = \int_a^b k(r) r dr. \quad (\text{A17})$$

The line element is dr , and the variance of the integrand is

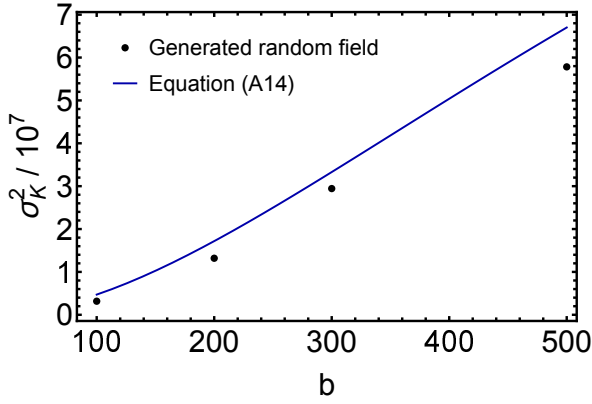


Figure A1. A comparison between the covariance of stochastically generated data (black dots) and that from Equation (A14) (blue curve).

$r^2 \sigma^2(k)$, so

$$\sigma^2(K) = \int_a^b r^2 \sigma^2(k) l(r) dr. \quad (\text{A18})$$

Similarly for a two-dimensional case, suppose

$$K = \int_0^{2\pi} d\phi \int_a^b k(r, \phi) r dr \quad (\text{A19})$$

and the correlation lengths of k is $l_r(r)$ and $l_\phi(r)$ in the radial and azimuthal directions, respectively. Note that the variance of

$$K_1(r) = \int_0^{2\pi} k(r, \phi) r d\phi \quad (\text{A20})$$

is just

$$\sigma^2(K_1) = \int_0^{2\pi} \sigma^2(k) l_\phi(r) r d\phi. \quad (\text{A21})$$

Then since $K = \int K_1(r) dr$, we obtain

$$\sigma^2(K) = \int_0^{2\pi} d\phi \int_a^b \sigma^2(k) l_r l_\phi r dr. \quad (\text{A22})$$

APPENDIX B: LUMINOSITY FLUCTUATIONS AND THEIR COHERENCE SCALES IN TIME AND FREQUENCY

At a given (non-dimensional) frequency β , fluctuations of the spectrum also have coherence time scales associated with different types of perturbations. For the IE this is simply the time scale of the external perturbation, and in our case, $\tau_{\text{IE}} = \tau_{\text{acc}}$. For the FE, the problem is more complex, again because the observed flux has non-local contributions from all radii, and the turbulent eddy turnover scales as $r^{3/2}$.

In the present work, we do not solve for the full statistics of the variability, but provide an upper limit to the coherence time. Assuming that photons at a specific frequency ν are emitted by a single annulus whose position \tilde{r}_β is determined by Wien's displacement law:

$$\frac{h_P \nu}{kT(\tilde{r}_\beta)} \simeq 2.8 \Rightarrow \beta = \frac{h_P \nu}{kT_*} = 2.8 \tilde{r}_\beta^{-21/40}, \quad (\text{B1})$$

the estimated upper limit of the coherence time of FE is then

$$\tau_{\text{FE}}(\beta) = \tau_{\text{ed}}(\tilde{r}_\beta) \simeq \Omega_K(\tilde{r}_\beta) = 18.9 \beta^{-20/7} \Omega_{K*}^{-1}. \quad (\text{B2})$$

Next we estimate the photon frequency range over which fluctuations in the disc spectrum are expected to be coherent. The coherence length of the temperature fluctuations l is propagated to a coherent frequency width $\Delta\beta$ by

$$\Delta\beta = \left| \frac{\partial\beta}{\partial\tilde{r}_\beta} \right| \frac{l}{r_*} \simeq 0.074 \beta^{61/21} \frac{l}{r_*}. \quad (\text{B3})$$

Taking $l = l_{\text{acc}}(\tilde{r}_\beta)$ [Equation (41)] or $l = l_{\text{ed}} = \alpha^{1/2} h(\tilde{r}_\beta)$ [Equation (31)] gives, respectively, the coherent frequency width associated with IE and FE in our model:

$$\frac{\Delta\beta_{\text{IE}}}{\beta} = 5 \times 10^{-5} \beta^{8/3} \left(\frac{\Omega_{K*} \tau_{\text{acc}}}{10^3} \right) \left(\frac{\alpha}{0.01} \right) \left(\frac{\theta}{0.01} \right)^2, \quad (\text{B4})$$

$$\frac{\Delta\beta_{\text{FE}}}{\beta} = 9 \times 10^{-6} \beta^{82/21} \left(\frac{\alpha}{0.01} \right)^{1/2} \left(\frac{\theta}{0.01} \right). \quad (\text{B5})$$

The above expressions and small values are likely overestimates because the disc emission at a given frequency has contributions from incoherent fluctuations at all annuli.

REFERENCES

- Abramowicz M. A., Czerny B., Lasota J. P., Szuszkiewicz E., 1988, *ApJ*, **332**, 646
- Ansdell M., et al., 2018, *ApJ*, **859**, 21
- Balbus S. A., Hawley J. F., 1991, *ApJ*, **376**, 214
- Balbus S. A., Hawley J. F., 1992, *ApJ*, **400**, 610
- Blackman E. G., 1998, *MNRAS*, **299**, L48
- Blackman E. G., Nauman F., Edgar R. G., 2010, arXiv e-prints, p. [arXiv:1010.1478](https://arxiv.org/abs/1010.1478)
- Bodo G., Cattaneo F., Mignone A., Rossi P., 2014, *ApJL*, **787**, L13
- Burd P. R., Kohlhepp L., Wagner S. M., Mannheim K., Buson S., Scargle J. D., 2020, arXiv e-prints, p. [arXiv:2010.12318](https://arxiv.org/abs/2010.12318)
- Churazov E., Gilfanov M., Revnitvsev M., 2001, *MNRAS*, **321**, 759
- Edelson R.,andra K., 1999, *ApJ*, **514**, 682
- Edgar R. G., Quillen A. C., Park J., 2007, *MNRAS*, **381**, 1280
- Flaherty K., et al., 2020, arXiv e-prints, p. [arXiv:2004.12176](https://arxiv.org/abs/2004.12176)
- Green A. R., McHardy I. M., Lehto H. J., 1993, *MNRAS*, **265**, 664
- Hawley J. F., Balbus S. A., 1991, *ApJ*, **376**, 223
- Hawley J. F., Balbus S. A., 1992, *ApJ*, **400**, 595
- Hawley J. F., Krolik J. H., 2001, *ApJ*, **548**, 348
- Hawley J. F., Gammie C. F., Balbus S. A., 1995, *ApJ*, **440**, 742
- Hoshino M., Takeshima T., 1993, *ApJL*, **411**, L79
- Ingram A., Done C., 2011, *MNRAS*, **415**, 2323
- King A. R., Pringle J. E., Livio M., 2007, *MNRAS*, **376**, 1740
- Kotko I., Lasota J. P., 2012, *A&A*, **545**, A115
- Kotov O., Churazov E., Gilfanov M., 2001, *MNRAS*, **327**, 799
- Lawrence A., Papadakis I., 1993, *ApJL*, **414**, L85
- Lee D., Gammie C. F., 2020, arXiv e-prints, p. [arXiv:2011.07151](https://arxiv.org/abs/2011.07151)
- Liu H. T., Bai J. M., Zhao X. H., Ma L., 2008, *ApJ*, **677**, 884
- Lyubarskii Y. E., 1997, *MNRAS*, **292**, 679
- Markowitz A., et al., 2003, *ApJ*, **593**, 96
- McHardy I. M., Papadakis I. E., Uttley P., Page M. J., Mason K. O., 2004, *MNRAS*, **348**, 783
- Mushtukov A. A., Ingram A., van der Klis M., 2018, *MNRAS*, **474**, 2259
- Mushtukov A. A., Lipunova G. V., Ingram A., Tsygankov S. S., Mönkkönen J., van der Klis M., 2019, *MNRAS*, **486**, 4061
- Narayan R., Yi I., 1994, *ApJL*, **428**, L13
- Narayan R., Yi I., 1995a, *ApJ*, **444**, 231
- Narayan R., Yi I., 1995b, *ApJ*, **452**, 710
- Nauman F., Blackman E. G., 2014, *MNRAS*, **441**, 1855

- Nauman F., Blackman E. G., 2017, *Physical Review E*, **95**, 033202
- Rafikov R. R., 2017, *ApJ*, **837**, 163
- Rapisarda S., Ingram A., Kalamkar M., van der Klis M., 2016, *MNRAS*, **462**, 4078
- Sano T., Inutsuka S.-i., Turner N. J., Stone J. M., 2004, *ApJ*, **605**, 321
- Shakura N. I., Sunyaev R. A., 1973, *A&A*, **500**, 33
- Shapiro S. L., Lightman A. P., Eardley D. M., 1976, *ApJ*, **204**, 187
- Shi J.-M., Stone J. M., Huang C. X., 2016, *MNRAS*, **456**, 2273
- Sorathia K. A., Reynolds C. S., Stone J. M., Beckwith K., 2012, *ApJ*, **749**, 189
- Stone J. M., Hawley J. F., Gammie C. F., Balbus S. A., 1996, *ApJ*, **463**, 656
- Uttley P., McHardy I. M., 2001, *MNRAS*, **323**, L26
- Vaughan S., Edelson R., Warwick R. S., Uttley P., 2003, *MNRAS*, **345**, 1271
- Velikhov E. P., 1959, *Sov. Phys. JETP*, **36**, 995
- Zhou H., Blackman E. G., Chamandy L., 2018, *Journal of Plasma Physics*, **84**, 735840302